

## Dynamic Clustering and Chemotactic Collapse of Self-Phoretic Active Particles

Oliver Pohl<sup>1</sup> and Holger Stark<sup>1,2</sup>

<sup>1</sup>*Institut für Theoretische Physik, Technische Universität Berlin, Hardenbergstrasse 36, 10623 Berlin, Germany*

<sup>2</sup>*Kavli Institute for Theoretical Physics, Kohn Hall, University of California, Santa Barbara, California 93106, USA*

(Received 13 March 2014; published 10 June 2014)

Recent experiments with self-phoretic particles at low concentrations show a pronounced dynamic clustering [I. Theurkauff *et al.*, *Phys. Rev. Lett.* **108**, 268303 (2012)]. We model this situation by taking into account the translational and rotational diffusiophoretic motion, which the active particles perform in their self-generated chemical field. Our Brownian dynamics simulations show pronounced dynamic clustering only when these two phoretic contributions give rise to competing attractive and repulsive interactions, respectively. We identify two dynamic clustering states and characterize them by power-law-exponential distributions. In case of mere attraction a chemotactic collapse occurs directly from the gaslike into the collapsed state, which we also predict by mapping our Langevin dynamics on the Keller-Segel model for bacterial chemotaxis.

DOI: 10.1103/PhysRevLett.112.238303

PACS numbers: 82.70.Dd, 05.10.Gg, 05.20.-y, 47.57.J-

The collective motion of self-propelling objects is a most fascinating subject that has been studied in a variety of systems [1,2]. At the macro scale, collective patterns occur, for example, in flocks of birds or fish schools [3–5], while at the microscopic scale bacterial cells in an aqueous environment generate intricate motional patterns [6–8]. To understand basic features of structure formation in non-equilibrium, systems with spherical or circular microswimmers are investigated. A number of theoretical and experimental studies have demonstrated that activity of microswimmers alone can result in clustering and phase separation [9–17] due to reduced motility in dense aggregates [9,15]. However, the colloidal density has to be large enough that the characteristic time for a particle to join a cluster becomes comparable to its rotational diffusion time needed to dissolve from it [13]. Other investigations explore the influence of hydrodynamics on collective motion [18–24].

In experiments with dilute suspensions of self-phoretic active Janus colloids, dynamic clustering has been observed [25,26]. In this novel nonequilibrium phenomenon, particles constantly join and leave clusters that exhibit a very dynamic shape. Since the colloids consume a chemical, they create a nonuniform chemical field around themselves. The chemical gradients initiate diffusiophoresis [27], whereby colloids can attract each other as demonstrated in Ref. [26]. The diffusiophoretic mechanism not only provides a novel colloidal interaction, it also serves as a biomimetic version of bacterial chemotaxis [28], where cells identify and swim along chemical gradients. Autochemotactic cells typically conglomerate in large aggregates or even exhibit a chemotactic collapse [7,29–32].

Recent theoretical and experimental studies included short-range attraction between active colloids and observed clustering at low colloidal densities [26,33–35]. Reference [36] implements diffusiophoresis for concrete

surface properties of self-phoretic colloids and identifies various states such as clumping and asters.

The work presented here has very much been inspired by the experiments of the Lyon group [25]. The diffusiophoretic interaction has a translational and orientational contribution. Using Brownian dynamics simulations, we demonstrate that pronounced dynamic clustering occurs only when these two contributions give rise to competing attractive and repulsive interactions, respectively. We identify two dynamic clustering states and characterize them. Otherwise, in case of mere attraction a chemotactic collapse occurs directly from the gaslike state before pronounced clusters are able to form. We support this result by mapping our Langevin dynamics on the Keller-Segel model for bacterial chemotaxis.

In our model we consider a dilute suspension of  $N$  self-phoretic colloids confined in a quadratic box. For example, by adding the chemical  $\text{H}_2\text{O}_2$ , they become active due to self-electrophoresis [37] and the colloids move with a swimming velocity  $v_0$ . It depends on the concentration  $c$  of the chemical that is a control parameter in the experiments [38,39]. We assume that  $v_0$  does not change noticeably due to local inhomogeneities of  $c$  and consider it as a system parameter [25,40]. In addition, the active colloids experience diffusiophoretic forces along chemical gradients, which are generated by the other colloids when they consume the chemical. Since the colloids are bipolar, a torque also aligns their swimming directions  $\mathbf{e}$  along a chemical gradient. The associated translational and rotational diffusiophoretic velocities are given by [27]

$$\mathbf{v}_D = [\langle \zeta \rangle \mathbf{1} - \langle \zeta (3\mathbf{n} \otimes \mathbf{n} - \mathbf{1}) / 2 \rangle] \nabla c, \quad (1)$$

$$\boldsymbol{\omega}_D = \frac{9}{4a} \langle \zeta \mathbf{n} \rangle \times \nabla c. \quad (2)$$

Here the slip-velocity coefficient  $\zeta$ , also called mobility constant in Ref. [41], depends on the interaction of the chemical with the colloid's surface,  $\langle \dots \rangle$  is an average over the surface with local normal vector  $\mathbf{n}$ , and  $a$  is the colloid radius. The quadrupolar term in Eq. (1) vanishes for half-coated colloids, whereas the angular velocity  $\boldsymbol{\omega}_D$  with  $\langle \zeta \mathbf{n} \rangle \propto \mathbf{e}_i$  is nonzero since the strength of the chemical-surface interaction and thereby the coefficient  $\zeta$  is different for the two halves of the Janus colloids [42]. Using  $\dot{\mathbf{e}}_i = \boldsymbol{\omega}_D \times \mathbf{e}_i$  and  $(\mathbf{e}_i \times \nabla c) \times \mathbf{e}_i = (\mathbf{1} - \mathbf{e}_i \otimes \mathbf{e}_i) \nabla c$ , we obtain a system of two Langevin equations describing the two-dimensional position  $\mathbf{r}_i$  and direction  $\mathbf{e}_i$  of the  $i$ th colloid in the overdamped limit,

$$\dot{\mathbf{r}}_i = v_0 \mathbf{e}_i - \zeta_{\text{tr}} \nabla c(\mathbf{r}_i) + \boldsymbol{\xi}_i, \quad (3)$$

$$\dot{\mathbf{e}}_i = -\zeta_{\text{rot}} (\mathbf{1} - \mathbf{e}_i \otimes \mathbf{e}_i) \nabla c(\mathbf{r}_i) + \boldsymbol{\mu}_i \times \mathbf{e}_i, \quad (4)$$

where we introduce  $\mathbf{e}_i := \langle \zeta \mathbf{n} \rangle / |\langle \zeta \mathbf{n} \rangle|$  and the respective translational and rotational diffusiophoretic parameters  $\zeta_{\text{tr}} := \langle \zeta \rangle$ ,  $\zeta_{\text{rot}} := 9 |\langle \zeta \mathbf{n} \rangle| / (4a)$ . Thermal and intrinsic fluctuations enter the equations by translational ( $\boldsymbol{\xi}_i$ ) and rotational ( $\boldsymbol{\mu}_i$ ) noise with zero mean and correlations  $\langle \boldsymbol{\xi}_i \otimes \boldsymbol{\xi}_i \rangle = 2D_{\text{tr}} \mathbf{1} \delta(t - t')$  and  $\langle \boldsymbol{\mu}_i \otimes \boldsymbol{\mu}_i \rangle = 2D_{\text{rot}} \mathbf{1} \delta(t - t')$ . We model the active particles as hard spheres; so, whenever they start to overlap, we separate them along the line connecting their centers. The chemical field diffuses and has sinks at the positions of the particles since they consume the chemical [43]:  $\dot{c}(\mathbf{r}) = D_c \nabla^2 c - k \sum_{i=1}^N \delta(\mathbf{r} - \mathbf{r}_i)$ . Since the chemical diffuses much faster than the colloids move, a stationary density field develops at each instance,

$$c(\mathbf{r}) = c_0 - \frac{k}{4\pi D_c} \sum_{i=1}^N \frac{1}{|\mathbf{r} - \mathbf{r}_i|}. \quad (5)$$

In experiments, active colloids settle on a surface and swim in two dimensions while the chemical field diffuses freely in half-space. Implementing zero flux at the surface by image colloids does not change the form of Eq. (5). The same holds when we integrate the concentration over a layer with thickness twice the colloid radius  $a$  to make the relevant concentration field two-dimensional.

Within clusters of active colloids, the concentration field cannot freely diffuse. So, whenever a colloid is surrounded by six closely packed neighbors, we introduce for it a screened chemical field  $\exp[-(r - \xi)/\xi]/r$ , with the screening length  $\xi = 2a(1 + \epsilon)$ . In our simulations we typically take  $\epsilon = 0.3$  and have checked that our results do not change when  $\epsilon$  is changed by 50%. We rescale time and length by  $t_r = 1/(2D_{\text{rot}})$  and  $l_r = \sqrt{D_{\text{tr}}/D_{\text{rot}}} = 2.33a$ , respectively. For historical reasons this is above the experimental value of  $1.79a$  [25], while the thermal value is  $1.15a$ . Again, the following results do not change drastically, if we adjust the value. The noise intensities for rescaled  $\boldsymbol{\xi}_i$  and  $\boldsymbol{\mu}_i$  become one and we are left with three essential parameters: the Péclet number

$\text{Pe} = v_0/(2\sqrt{D_{\text{tr}}D_{\text{rot}}})$  and reduced translational as well as rotational diffusiophoretic parameters  $\zeta_{\text{tr}}k/(8\pi D_{\text{tr}}D_c) \rightarrow \zeta_{\text{tr}}$  and  $\zeta_{\text{rot}}k/(8\pi D_c\sqrt{D_{\text{tr}}D_{\text{rot}}}) \rightarrow \zeta_{\text{rot}}$ , respectively, for which we keep the same symbols.

Note that in our model each active colloid creates a chemical sink. So, for  $\zeta_{\text{tr}} > 0$  and  $\zeta_{\text{rot}} > 0$  it pulls and rotates other colloids towards itself, which means an effective attraction. At boundaries of the simulation box, we let colloids move with a randomly chosen direction back into the box. Following experiments [25], we investigate dilute systems with an area fraction of  $\sigma = 5\%$  and simulate a total of 800 particles. We have checked that a larger number does not change our results qualitatively as long as the area fraction is maintained. Finally, we choose the swimming velocity  $v_0$  in the range 2–4.5  $\mu\text{m/s}$  as in experiments [25] corresponding to Péclet numbers  $\text{Pe} = 10$ –22.

In Fig. 1 we illustrate typical particle configurations for increasing translational diffusiophoretic parameter  $\zeta_{\text{tr}}$ . At  $\zeta_{\text{tr}} = 0$  (upper left) the active colloids hardly cluster since there is no phoretic attraction between them. They assume a gaslike state with a mean cluster size  $N_c$  close to 3. To determine  $N_c$ , we define a cluster as an assembly of more than two colloids and average over many snapshots at different times. Thus, by definition  $N_c \geq 3$ . In contrast, at large  $\zeta_{\text{tr}}$  (bottom right) the system collapses into a single large cluster similar to the chemotactic collapse that occurs in bacterial systems [29,44]. In between, we observe dynamic clustering (top right, bottom left). Motile clusters form that strongly fluctuate in shape and size and ultimately dissolve again (see movies 1 and 2 in the Supplemental

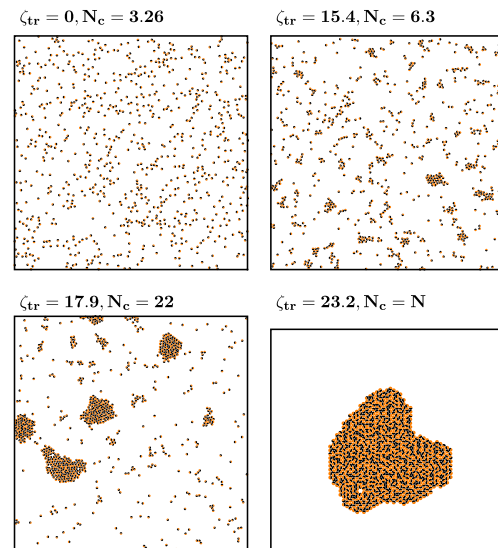


FIG. 1 (color online). Snapshots of colloid configurations for increasing  $\zeta_{\text{trans}}$  at  $\zeta_{\text{rot}} = -0.38$  and  $\text{Pe} = 19$ . Top left: gaslike state. Top right: dynamic clustering 1. Bottom left: dynamic clustering 2. Bottom right: collapsed state.  $N_c$  is the mean cluster size.

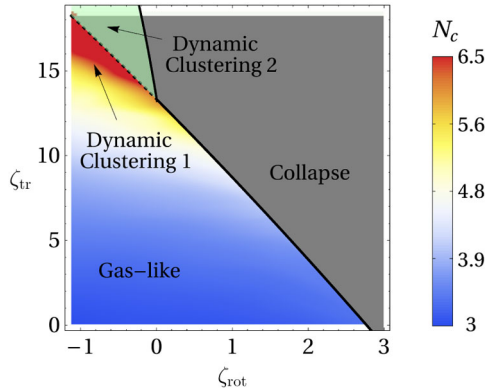


FIG. 2 (color online). State diagram:  $\zeta_{tr}$  versus  $\zeta_{rot}$  at  $Pe = 19$ . The mean cluster size  $N_c$  is color coded.

Material [45]). In Fig. 2 we plot a state diagram in the phoretic parameters  $\zeta_{tr}$ ,  $\zeta_{rot}$ , where we also color code the mean cluster size  $N_c$ . At  $\zeta_{rot} = 0$  the maximal dynamic cluster size just before the collapse is  $N_c \approx 5$ . When we turn on rotational diffusiophoresis with  $\zeta_{rot} > 0$ , the swimming direction  $\mathbf{e}$  of a free active colloid points towards a cluster (chemical sink), which further supports the formation of one cluster. This explains the fact that in Fig. 2 the collapse occurs for smaller  $\zeta_{tr}$  when  $\zeta_{rot}$  increases. The mean cluster size just before the collapse decreases and dynamic clustering is hardly visible. In contrast, at  $\zeta_{rot} < 0$  active particles rotate away from chemical sinks and thus an effective repulsion is introduced. Once active colloids join a cluster, their swimming direction rotates outwards and the colloids can leave the cluster again if the translational phoretic attraction is not too large. This balance of effective phoretic attraction and repulsion is the cause for pronounced dynamical clustering with large cluster sizes. Interestingly, the state diagram in Fig. 2 indicates two clustering states: one where cluster sizes up to 6.5 are observed (see snapshot at top right in Fig. 1) and a second clustering state where much larger dynamic clusters occur (see snapshot at bottom left in Fig. 1).

To further quantify the two dynamic clustering states 1 and 2, we determine the cluster-size distribution  $P(n)$ . In Fig. 3 we plot it for fixed rotational phoretic parameter  $\zeta_{rot} = -0.38$  and increasing translational coupling  $\zeta_{tr}$ . For pure steric interaction ( $\zeta_{tr} = 0$ , blue curve), an exponential decay is predominant. Closer to the transition line between dynamic clustering states 1 and 2 in Fig. 2, the distribution follows a power law at small  $n$ , before it falls off exponentially (orange and red curves in Fig. 3). Indeed, we can fit our results by  $P(n) = c_0 n^{-\beta} \exp(-n/n_0)$  with exponent  $\beta = 2.1 \pm 0.1$ , which gradually decreases for more negative  $\zeta_{rot}$ . This fit is robust against increasing particle number as demonstrated in the Supplemental Material [45]. With further increase of  $\zeta_{tr}$  we observe that the distribution  $P(n)$  develops an inflection point (green curves) and we have to use a sum of two power-law-exponential curves to fit our distributions,  $P(n) = c_1 n^{-\beta_1} \exp(-n/n_1) + c_2 n^{-\beta_2} \exp(-n/n_2)$  with  $\beta_1 = 2.1 \pm 0.2$  and  $\beta_2 \approx 1.5$ .

This defines the dynamic clustering state 2, where very large clusters coexist with smaller ones and individual particles. The transition in the cluster-size distribution is observed for all negative  $\zeta_{rot}$ . Typically, the mean cluster size  $N_c$  increases strongly in state 2 as indicated in the inset of Fig. 3. In contrast, for  $\zeta_{rot} > 0$  the system exhibits the collapse to a single cluster before large dynamic clusters can appear. When we turn off screening of the chemical field within clusters, the clustering state 2 disappears completely as demonstrated in the Supplemental Material [45].

Similar cluster-size distributions including the transition indicated by the occurrence of an inflection point have been observed in experiments on gliding bacteria [7]. However, in this work bacterial density was varied in a system with pure hard-core interactions causing nematic alignment. In contrast, we vary the strength of the diffusiophoretic coupling ultimately leading to the collapsed state, which has not been observed in Ref. [7].

The experiments with diffusiophoretic coupling showed a linear scaling of the mean cluster size with  $Pe$ :  $N_c \sim Pe$  [25]. It appears counterintuitive that at low area fractions of  $\sigma = 5\%$  faster colloids generate larger clusters and indeed the simulations of our model show the contrary behavior. In Fig. 4 we plot a state diagram in  $\zeta_{tr}$  versus  $Pe$  while  $\zeta_{rot}$  is kept constant. Clearly, for constant  $\zeta_{tr}$  large clusters disappear with increasing  $Pe$ . However, large activity  $Pe$  is necessary for observing dynamic clustering. At small  $Pe$  only small cluster sizes occur with increasing  $\zeta_{tr}$ , while at sufficiently large  $Pe$  we observe both dynamic clustering states.

In the experiments of Ref. [25] colloidal activity increases with the concentration  $c_0$  of the activating chemical  $H_2O_2$ . According to Ref. [39], the swimming velocity scales as  $c_0 \sim v_0 \propto Pe$ . The concentration  $c$  also couples to our reparametrized diffusiophoretic parameters  $\zeta_{tr}$  and  $\zeta_{rot}$  through the reaction rate  $k$  introduced in Eq. (5). In the following, we assume Michaelis-Menten kinetics for the reaction rate in the linear regime well before saturation,  $k \sim c_0$ , and thus find  $\zeta_{tr} \sim c_0 \sim \zeta_{rot}$ . So, the linear

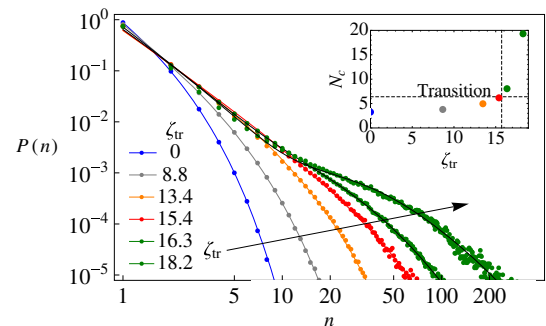


FIG. 3 (color online). Cluster-size distributions  $P(n)$  for increasing translational phoretic parameter  $\zeta_{tr}$  at  $Pe = 19$  and  $\zeta_{rot} = -0.38$ .  $\zeta_{tr}$  assumes the values 0, 8.8, 14.5, 15.4, 16.3, and 18.2. The transition between dynamic clustering states 1 and 2 occurs between the red and green curves. Inset: mean cluster size  $N_c$  versus  $\zeta_{tr}$ . The transition is indicated.

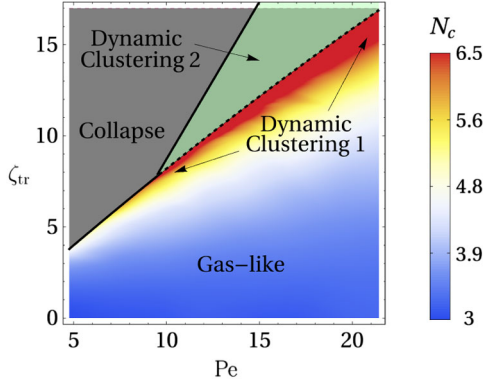


FIG. 4 (color online). State diagram plotting mean cluster size  $N_c$  against Péclet number  $Pe$  and chemotactic control parameter  $\zeta_{tr}$ .  $\zeta_{rot} = -0.38$ . The color code indicates the mean number of particles  $N_c$  in a dynamic cluster.

dependence of the parameters  $Pe$ ,  $\zeta_{tr}$ , and  $\zeta_{rot}$  on  $c_0$  defines a line in the parameter space. In this space the dynamic clustering states 1 and 2 are separated by a plane. We choose different lines that always hit the transition plane and plot in Fig. 5 the mean cluster size  $N_c$  versus  $Pe$  along the lines. The blue and purple curves show the strong increase of  $N_c$  when the clustering state 2 is entered, since the respective lines hit the transition plane under angles closer to  $90^\circ$ . Making this angle smaller, the increase is more modest. In particular, the green graph shows an almost linear increase of  $N_c$  in the  $Pe$  range from 10 to 20. So, Fig. 5 demonstrates that the relation between  $N_c$  and swimming velocity does not have a simple dependence.

To gain some more insight into the transition to the collapsed state, we formulate a Smoluchowski equation for the full spatial and orientational probability distribution. We determine its orientational moments and derive an equation for the spatial colloidal density  $P(\mathbf{r}, t)$  coupled to the chemical field  $c(\mathbf{r}, t)$ , similar to the approach in Ref. [46,47]:  $\dot{P} = \zeta_{eff} \nabla \cdot (P \nabla c) + D_{eff} \nabla^2 P + O((\nabla c)^2)$ .

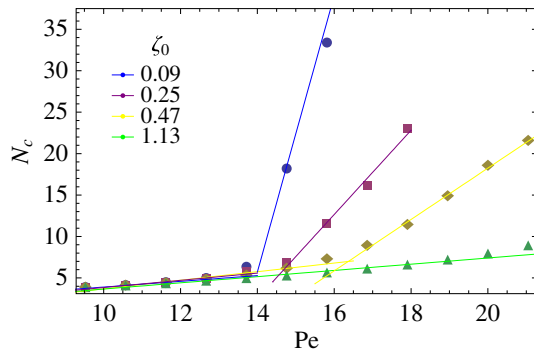


FIG. 5 (color online). Mean cluster size  $N_c$  versus  $Pe$  for different lines in the full parameter space defined via a parametrization with  $x \in [0, 1]$ . We vary  $Pe$  as in experiments of Ref. [25],  $Pe = 9.5 + 11.5x$ , and choose  $\zeta_{tr} = 4.8 + 16.6x$  and  $\zeta_{rot} = -0.16 - \zeta_0 x$ , where the parameter  $\zeta_0$  defines the different graphs. The transition between clustering states 1 and 2 roughly occurs at the intersection of the two straight lines.

Details are given in the Supplemental Material [45]. This equation is reminiscent of one relation of the Keller-Segel model [29] used to describe the chemotaxis of bacteria but here with effective chemotactic and diffusion constants:  $\zeta_{eff} = \zeta_{tr} + (\zeta_{rot} v_0 / 2D_{rot})$  and  $D_{eff} = D_{tr} + (v_0^2 / 2D_{rot})$ . In two dimensions it exhibits an instability of the uniform state towards a chemotactic collapse when its parameters satisfy  $(\zeta_{eff} k \sigma / D_c D_{eff}) > b$ , where  $\sigma$  is the area fraction of the colloids and  $b$  is a constant that depends on the geometry of the system [44,48]). In our unitless parameters the condition becomes  $8\pi\sigma(\zeta_{tr} + \zeta_{rot} Pe) / (1 + 2Pe^2) > b$ . For constant  $Pe$ , this agrees nicely with the nearly straight transition line in Fig. 2 between the gaslike and the collapsed state at  $\zeta_{rot} > 0$ . However, the condition does not reproduce the straight transition line in Fig. 4. The reason is that at  $\zeta_{rot} < 0$  pronounced clustering occurs before the collapse takes place. In the Supplemental Material [45] we test the collapse condition in regions where dynamic clustering is absent ( $\zeta_{rot} > 0$ ). Dynamic clustering, however, cannot be described by the Keller-Segel equation. Clustering occurs when a colloid moves towards the rim of a cluster and rotates away from it ( $\zeta_{rot} < 0$ ), and then a delicate balance between swimming away from the cluster and diffusiophoretic attraction by the cluster sets in:  $v_0 \sim \zeta_{tr} |\nabla c|$ . This mechanism crucially depends on ballistic swimming with velocity  $v_0$ . It cannot be described by our Keller-Segel equation since  $v_0$  only appears in effective chemotactic and diffusion parameters. Assuming that the colloid attaches directly to two particles at the rim of a cluster, we estimate in our reduced units  $|\nabla c| \approx 1 / (2a / 2.33a)^2 = 1 / 0.73$  and obtain a condition for dynamic clustering:  $\zeta_{tr} \approx 0.73 Pe$ . This simple estimate reproduces the straight transition line between clustering states 1 and 2 in Fig. 4 and the region where clustering occurs. A more thorough explanation of dynamic clustering might use the kinetic approach of Refs. [7,49] but this is beyond the scope of this Letter.

To conclude, self-phoretic active colloids mediate diffusiophoretic interactions between each other. They consist of a translational and an orientational part, which together with the active swimming can act either attractively or repulsively. When they are both attractive, the colloids show a transition from the gaslike to a collapsed state reminiscent of a chemotactic collapse in bacterial systems as our mapping on the Keller-Segel model demonstrates. When translational and rotational diffusiophoresis generate counteracting attraction and repulsion, two dynamic clustering states with characteristic cluster-size distributions are stabilized similar to the dynamic clustering observed in the experiments of Ref. [25].

The present system mimics chemotaxis in bacterial colonies without relying on a complex signalling pathway necessary in cells. Thereby, it may help to explore chemotactic structure formation and design novel dynamic patterns in bacterial colonies [6].

We thank M. Bär, L. Bocquet, F. Peruani, C. Prohm, C. Valeriani, and K. Wolff for helpful discussions and one referee for bringing Ref. [41] to our attention. We also acknowledge funding from the DFG within the research training group GRK 1558. This research was supported in part by the National Science Foundation under Grant No. PHY11-25915. H.S. thanks the Kavli Institute for Theoretical Physics for hospitality and financial support.

- 
- [1] T. Vicsek and A. Zafeiris, *Phys. Rep.* **517**, 71 (2012).
- [2] M. C. Marchetti, J.-F. Joanny, S. Ramaswamy, T. B. Liverpool, J. Prost, M. Rao, and R. S. Simha, *Rev. Mod. Phys.* **85**, 1143 (2013).
- [3] M. Ballerini, N. Calibbio, R. Candeir, A. Cavagna, E. Cisbani, I. Giardina, V. Lecomte, A. Orlandi, G. Parisi, A. Procaccini, M. Viale, and V. Zdravkovic, *Proc. Natl. Acad. Sci. U.S.A.* **105**, 1232 (2008); A. Cavagna, A. Cimarelli, I. Giardina, G. Parisi, R. Santagati, F. Stefanini, and M. Viale, *Proc. Natl. Acad. Sci. U.S.A.* **107**, 11865 (2010).
- [4] W. Bialek, A. Cavagna, I. Giardina, T. Mora, O. Pohl, E. Silvestri, M. Viale, and A. Walczak, [arXiv:1307.5563](https://arxiv.org/abs/1307.5563).
- [5] N. C. Makris, P. Ratilal, D. T. Symonds, S. Jagannathan, S. Lee, and R. W. Nero, *Science* **311**, 660 (2006); Y. Katz, C. C. Ioannou, K. Tunstro, C. Huepe, and I. D. Couzin, *Proc. Natl. Acad. Sci. U.S.A.* **108**, 18720 (2011).
- [6] J. Saragostia, V. Calvez, N. Bournaveas, B. Perthame, A. Buguin, and P. Silberzan, *Proc. Natl. Acad. Sci. U.S.A.* **108**, 16235 (2011).
- [7] F. Peruani, J. Starrau, V. Jakovljevic, L. Sogaard-Andersen, A. Deutsch, and M. Bär, *Phys. Rev. Lett.* **108**, 098102 (2012).
- [8] H. H. Wensink, J. Dunkel, S. Heidenreich, K. Drescher, R. E. Goldsteinc, H. Löwen, and J. M. Yeomans, *Proc. Natl. Acad. Sci. U.S.A.* **109**, 14308 (2012).
- [9] J. Tailleur and M. E. Cates, *Phys. Rev. Lett.* **100**, 218103 (2008).
- [10] S. Henkes, Y. Fily, and M. C. Marchetti, *Phys. Rev. E* **84**, 040301 (2011).
- [11] Y. Fily and M. C. Marchetti, *Phys. Rev. Lett.* **108**, 235702 (2012).
- [12] J. Bialké, T. Speck, and H. Löwen, *Phys. Rev. Lett.* **108**, 168301 (2012).
- [13] G. S. Redner, M. F. Hagan, and A. Baskaran, *Phys. Rev. Lett.* **110**, 055701 (2013).
- [14] I. Buttinoni, J. Bialke, F. Kümmel, H. Löwen, C. Bechinger, and T. Speck, *Phys. Rev. Lett.* **110**, 238301 (2013).
- [15] M. E. Cates and J. Tailleur, *Europhys. Lett.* **101**, 20010 (2013).
- [16] J. Bialké, H. Löwen, and T. Speck, *Europhys. Lett.* **103**, 30008 (2013).
- [17] J. Stenhammar, A. Tiribocchi, R. J. Allen, D. Marenduzzo, and M. E. Cates, *Phys. Rev. Lett.* **111**, 145702 (2013).
- [18] T. Ishikawa and T. J. Pedley, *Phys. Rev. Lett.* **100**, 088103 (2008).
- [19] A. A. Evans, T. Ishikawa, T. Yamaguchi, and E. Lauga, *Phys. Fluids* **23**, 111702 (2011).
- [20] S. Thutupalli, R. Seemann, and S. Herminghaus, *New J. Phys.* **13**, 073021 (2011).
- [21] S. Fielding, [arXiv:1210.5464](https://arxiv.org/abs/1210.5464).
- [22] F. Alarcon and I. Pagonabarraga, *J. Mol. Liq.* **185**, 56 (2013).
- [23] J. J. Molina, Y. Nakayama, and R. Yamamoto, *Soft Matter* **9**, 4923 (2013).
- [24] A. Zöttl and H. Stark, *Phys. Rev. Lett.* **112**, 118101 (2014).
- [25] I. Theurkauff, C. Cottin-Bizonne, J. Palacci, C. Ybert, and L. Bocquet, *Phys. Rev. Lett.* **108**, 268303 (2012).
- [26] J. Palacci, S. Sacanna, A. P. Steinberg, D. J. Pine, and P. M. Chaikin, *Science* **339**, 936 (2013).
- [27] J. L. Anderson, *Annu. Rev. Fluid Mech.* **21**, 61 (1989).
- [28] H. C. Berg, *E. Coli in Motion* (Springer-Verlag, New York, 2004).
- [29] E. F. Keller and L. A. Segel, *J. Theor. Biol.* **26**, 399 (1970).
- [30] M. P. Brenner, L. S. Levitov, and E. O. Budrene, *Biophys. J.* **74**, 1677 (1998).
- [31] N. Mittal, E. O. Budrene, M. P. Brenner, and A. van Oudenaarden, *Proc. Natl. Acad. Sci. U.S.A.* **100**, 13259 (2003).
- [32] J. Taktikos, V. Zaburdaev, and H. Stark, *Phys. Rev. E* **84**, 041924 (2011).
- [33] B. M. Mognetti, A. Šaric, S. Angioletti-Uberti, A. Cacciuto, C. Valeriani, and D. Frenkel, *Phys. Rev. Lett.* **111**, 245702 (2013).
- [34] G. S. Redner, A. Baskaran, and M. F. Hagan, *Phys. Rev. E* **88**, 012305 (2013).
- [35] J. Schwarz-Linek, C. Valeriani, A. Cacciuto, M. E. Cates, D. Marenduzzo, A. N. Morozov, and W. C. K. Poon, *Proc. Natl. Acad. Sci. U.S.A.* **109**, 4052 (2012).
- [36] S. Saha, R. Golestanian, and S. Ramaswamy, [arXiv:1309.4947](https://arxiv.org/abs/1309.4947).
- [37] W. F. Paxton, A. Sen, and T. E. Mallouk, *Chem. Eur. J.* **11**, 6462 (2005).
- [38] J. L. Moran and J. Posner, *J. Fluid Mech.* **680**, 31 (2011).
- [39] J. L. Moran, P. M. Wheat, and J. D. Posner, *Phys. Rev. E* **81**, 065302 (2010).
- [40] In the experiments of Ref. [25] a 20-fold increase of the chemical was needed to increase  $v_0$  by a factor of about 2.5. Thus small inhomogeneities of the chemical field do not strongly alter the activity of the colloids.
- [41] T. Bickel, G. Zecua, and A. Würger, *Phys. Rev. E* **89**, 050303(R) (2014).
- [42] In Ref. [41] the translational and rotational diffusiophoretic velocities were calculated explicitly for Janus colloids assuming the two slip-velocity coefficients  $\zeta_1$  and  $\zeta_2$  for each side:  $\mathbf{v} = \langle \zeta \rangle \nabla c = [(\zeta_1 + \zeta_2)/2] \nabla c$  and  $\boldsymbol{\omega} = (9/4a) \langle \zeta \mathbf{n} \rangle \times \nabla c = (9/8a) (\zeta_1 - \zeta_2) \mathbf{e} \times \nabla c$ . Note, in contrast to Ref. [41] we do not explicitly treat self-propulsion of a colloid due to its own nonuniform field. Instead, the active colloids move with a given swimming velocity  $v_0$  as described in the paragraph before Eq. (1).
- [43] For simplicity, we just consider one chemical field and do not distinguish between reactants and products of the reaction catalyzed by the active particle.
- [44] W. Jäger and S. Luckhaus, *Trans. Am. Math. Soc.* **329**, 819 (1992).
- [45] See the Supplemental Material at <http://link.aps.org/supplemental/10.1103/PhysRevLett.112.238303> for a study of how the dynamic clustering state I depends on system size, state diagrams without chemical screening in the clusters, a derivation of the Keller-Segel equation, a test of the chemotactic collapse condition, and videos of dynamic clustering.
- [46] R. Golestanian, *Phys. Rev. Lett.* **108**, 038303 (2012).
- [47] K. Wolff, A. M. Hahn, and H. Stark, *Eur. Phys. J. E* **36**, 43 (2013).
- [48] M. A. Herrero and J. J. L. Velazquez, *J. Math. Biol.* **35**, 177 (1996).
- [49] F. Peruani and Markus Bär, *New J. Phys.* **15**, 065009 (2013).